

Current-voltage characteristics of a graphene nanoribbon field-effect transistor

V. Ryzhii[*], M. Ryzhii, and A. Satou

*Computer Solid State Physics Laboratory, University of Aizu, Aizu-Wakamatsu, 965-8580, Japan and
Japan Science and Technology Agency, CREST, Tokyo 107-0075, Japan*

T. Otsuji

*Research Institute for Electrical Communication,
Japan Science and Technology Agency, CREST, Tokyo 107-0075, Japan*

(Dated: November 2, 2018)

We present an analytical device model for a field-effect transistor based on a heterostructure which consists of an array of nanoribbons clad between the highly conducting substrate (the back gate) and the top gate controlling the source-drain current. The equations of the model of a graphene nanoribbon field-effect transistor (GNR-FET) include the Poisson equation in the weak nonlocality approximation. Using this model, we find explicit analytical formulas for the spatial distributions of the electric potential along the channel and for the GNR-FET current-voltage characteristics (the dependences of the source-drain current on the drain voltages as well as on the back gate and top gate voltages) for different geometric parameters of the device. It is shown that the shortening of the top gate can result in a substantial modification of the GNR-FET current-voltage characteristics.

I. INTRODUCTION

Graphene, i.e., a monolayer of carbon atoms forming a dense honeycomb two-dimensional (2D) crystal structure is considered as a promising candidate for future micro- and nanoelectronics [1, 2, 3, 4, 5]. The features of the electron and hole energy spectra in graphene provide the exceptional properties of graphene-based heterostructures and devices, in particular field-effect transistors [4, 6]. Fabrication and experimental studies as well as a theoretical model of graphene field-effect transistor (G-FET) was reported recently in, for instance, Ref. [6]. The operation of G-FETs is accompanied by the formation of the lateral n-p-n (or p-n-p) junction under the controlling (top) gate and the pertinent energy barrier. The current through this barrier can be associated by both thermionic and tunneling processes [6, 7, 8, 9, 10]. The utilization of the patterned graphene which constitutes an array of sufficiently narrow graphene strips (nanoribbons) provides an opportunity to engineer the band structure to achieve the optimal device parameters. In particular, properly choosing the width of the nanoribbons, one can fabricate the graphene structures with relatively wide band gap but rather high electron (hole) mobility [4, 11].

In this paper, we present an analytical device model for a graphene-nanoribbon FET (GNR-FET) and obtain the device characteristics. The GNR-FET under consideration is based on a patterned graphene layer which constitutes a dense array of parallel nanoribbons of width d with the spacing between the nanoribbons $d_s \ll d$. The nanoribbon edges are connected to the conducting pads serving as the transistor source and drain. A highly conducting substrate plays the role of the back gate, whereas the top gate serves to control the source-drain current. The device structure is schematically shown in Fig. 1. Using the developed model, we calculate the potential distributions in the GNR-FET as a function of the back

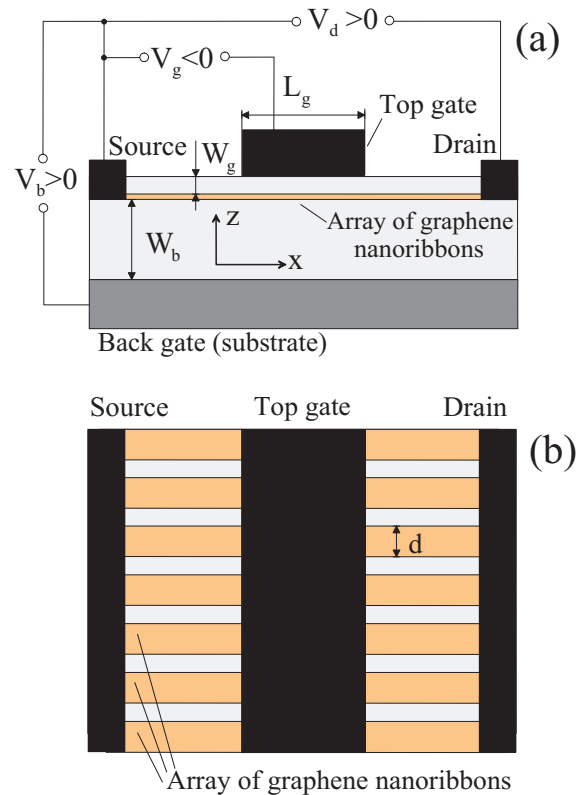


FIG. 1: Schematic side (a) and top (b) views of a GNR-FET structure.

gate, top gate, and drain voltages, V_b , V_g , and V_d (reckoned from the potential of the source contact), respectively, and the GNR-FET dc characteristics. This corresponds to a GNR-FET in the common-source circuit. The case of common drain will briefly be discussed as well. For the sake of definiteness, the back gate voltage V_b and the top gate voltage V_g are assumed to be, re-

spectively, positive and negative ($V_b > 0$ and $V_g < 0$) with respect to the potential of the source contact, so we consider GNR-FETs with the channel of n-type.

The paper is organized as follows. In Sec. II, the GNR-FET model is considered and the main equation governing the spatial distributions of the electric potential in the active region of the transistor channel is given. This equation is a consequence of the two-dimensional Poisson equation in the weak nonlocality approximation [10, 12, 13]. Section III deals with the derivation of the relations between the electron and hole densities in the channel and the electric potential and the consequent calculations of the potential spatial distributions depending on the drain and gate (back gate and top gate) voltages. In Sec. IV, using the obtained formulas for the electric potential and the height of the barrier for electrons at the minimum of the potential, we obtain analytical expressions for the source-drain current as a function of the drain and gate voltages. In Sec. V, we discuss the specific of GNR-FET operation in the circuits with common drain, the possible role of holes, and the limitations of the model used. In Sec. VI, we draw the main results.

II. GNR-FET MODEL

Graphene strips (nanoribbons) exhibit the energy spectrum with a gap between the valence and conduction bands depending on the nanoribbon width d :

$$\varepsilon_{p,n}^\mp = \pm v \sqrt{p^2 + (\pi\hbar/d)^2 n^2}. \quad (1)$$

Here $v \simeq 10^8$ cm/s is the characteristic velocity of the electron (upper sign) and hole (lower sign) spectra, p is the momentum in along the nanoribbon, \hbar is the reduced Planck constant, and $n = 1, 2, 3, \dots$ is the subband index. The quantization corresponding to Eq. (1) of the electron and hole energy spectra in nanoribbons due to the electron and hole confinement in one of the lateral directions results in the appearance of the band gap between the valence and conduction bands and in a specific the density of states (DOS) as a function of the energy.

The electron density in different parts of the channel and, therefore, the degree of the electron gas degeneration essentially depend on the back gate voltage. In contrast to graphene with zero energy gap, the electron (hole) gas in relatively narrow nanoribbons with quantized energy spectrum and the pertinent energy gap between the subbands in the valence and conduction band, can become degenerate at fairly high back gate voltages. In the following, we restrict ourselves by the consideration of the GNR-FET operation under the condition that the electron gas in the channel is nondegenerate. Such a consideration is valid in the voltage range which is sufficiently wide in terms of practical applications. Thus, the back gate voltage is assumed to be not excessively high, so that the electron density is moderate, the electron gas in the channel is nondegenerate, and the electrons occupy only the lowest ($n = 1$) subband in the conduction

band nanoribbons. Notwithstanding this, it is suggested that the channel sections adjacent to the source and drain contacts are highly conducting, so that these section are equipotential. The potentials are equal to the potentials of the source and drain contacts, i.e., equal to $\varphi = 0$ and $\varphi = V_d$, respectively.

We shall consider the GNR-FET region under the top gate (the device active region) defined as follows: $-L_g \leq x \leq L_g/2$, $-W_b \leq z \leq W_g$, where L_g is the length of the top gate, and W_b and W_g are the thicknesses of the layers between graphene and the back and top gates, respectively. Here, the axis x is directed along the nanoribbons, whereas the axis z is directed perpendicular to the nanoribbons and gate planes.

To find the potential distribution along the channel, we use the following equation:

$$\frac{(W_b + W_g)}{3} \frac{d^2 \varphi}{dx^2} - \frac{\varphi - V_b}{W_b} - \frac{\varphi - V_g}{W_g} = \frac{4\pi e}{\varepsilon} (\Sigma_- - \Sigma_+) \quad (2)$$

with the boundary conditions

$$\varphi|_{x=-L_g/2} = 0, \quad \varphi|_{x=L_g/2} = V_d. \quad (3)$$

Here, Σ_- and Σ_+ are the electron and hole sheet densities in the channel, e is the electron charge, and ε is the dielectric constant of the material separating the channel from the gates. Equation (2), which governs the electric potential, $\varphi = \varphi(x) = \psi(x, 0)$, in the channel is a consequence of the two-dimensional Poisson equation for the electric potential $\psi = \psi(x, z)$ for the active region under consideration in the weak nonlocality approximation [12, 13]. This equation provides solutions, which can be obtained from the exact solution of the two-dimensional Poisson by the expansion in powers of the parameter $\delta = [(W_b^3 + W_g^3)/45(W_b + W_g)\mathcal{L}^2]$, which is much smaller than unity in the situation under consideration. Here \uparrow is the characteristic scale of the lateral inhomogeneities (see Sec. V). The lowest approximation in such an expansion corresponds to the so-called gradual channel approximation proposed by W. Shockley, in which the first term in the left-hand side of Eq. (2) is neglected [14, 15], so that the relationship between the potential in the channel and the electron and hole charge becomes local. Thus, Eq. (2) can be used when $\delta < 1$ and, hence, when $\mathcal{L} \gtrsim \max\{W_b, W_g\}$. The harnessing of the approximation under consideration makes, in particular, possible to study essentially nonuniform potential distributions in the GNR-FET channel and the short-gate effects analytically. The weak nonlocality approximation was effectively used previously in some previous papers (see, for instance, Refs. [10, 12, 13, 16]).

Since the spacing, d_s between the nanoribbons is small, we disregard a small scale nonuniformity of the electric potential distribution in the in-plane direction y .

III. POTENTIAL DISTRIBUTIONS

The application of negative top gate voltage leads to the formation of a potential barrier in the channel under this gate. This barrier determined by the gate voltage controls the source-drain current and, hence, is responsible of the device operation as a transistor.

A. Electron and hole densities

Considering that the electron and hole gases are non-degenerate, and, hence, the electron and hole distribution functions in the subbands with $n = 1$ near the source and drain is given by

$$f_p^\mp \simeq \exp\left(\frac{\pm e\varphi \pm \varepsilon_F - \sqrt{v^2 p^2 + \Delta^2/4}}{k_B T}\right),$$

where ε_F is the Fermi energy reckoned from the middle of the energy band gap and $\Delta = \varepsilon_{0,1}^+ - \varepsilon_{0,1}^- = 2\pi v\hbar/d$ is the value of the energy band gap, the electric potential, the electron densities and the Fermi energies in the source and drain regions (marked by superscripts “s” and “d”, respectively) are related to each other as

$$\begin{aligned} \Sigma_{\mp}^s &= \frac{4k_B T}{\pi\hbar d v} \exp\left(\pm \frac{\varepsilon_F^s + e\varphi}{k_B T}\right) \int_{\xi_m}^{\infty} \frac{d\xi \xi \exp(-\xi)}{\sqrt{\xi^2 - \xi_m^2}} \\ &= \frac{2\Delta}{\pi\hbar d v} \exp\left(\pm \frac{\varepsilon_F^s + e\varphi}{k_B T}\right) K_1\left(\frac{\Delta}{2k_B T}\right), \end{aligned} \quad (4)$$

$$\begin{aligned} \Sigma_{\mp}^d &= \frac{4k_B T}{\pi\hbar d v} \exp\left[\pm \frac{\varepsilon_F^d + e(\varphi - V_d)}{k_B T}\right] \int_{\xi_m}^{\infty} \frac{d\xi \xi \exp(-\xi)}{\sqrt{\xi^2 - \xi_m^2}} \\ &= \frac{2\Delta}{\pi\hbar d v} \exp\left[\pm \frac{\varepsilon_F^d + e(\varphi - V_d)}{k_B T}\right] K_1\left(\frac{\Delta}{2k_B T}\right). \end{aligned} \quad (5)$$

Here, $\xi_m = \Delta/2k_B T$ and $K_1(\xi)$ is the modified Bessel function. Taking into account the asymptotic behavior of the Bessel function at $\xi \gg 1$, namely, $K_1(\xi) \simeq (\pi/2\xi)^{1/2} \exp(-\xi)$, for $\Delta \gg 2k_B T$, we obtain

$$\begin{aligned} \Sigma_{\mp}^s &\simeq \frac{2\sqrt{\Delta k_B T}}{\sqrt{\pi}\hbar d v} \exp\left(\pm \frac{\varepsilon_F^s + e\varphi}{k_B T} - \frac{\Delta}{2k_B T}\right), \\ \Sigma_{\mp}^d &\simeq \frac{2\sqrt{\Delta k_B T}}{\sqrt{\pi}\hbar d v} \exp\left[\pm \frac{\varepsilon_F^d + e(\varphi - V_d)}{k_B T} - \frac{\Delta}{2k_B T}\right]. \end{aligned} \quad (6)$$

Considering that when $\varphi = 0$ and $\varphi = V_d$, $\Sigma_{-,0}^s - \Sigma_{+,0}^s = \varepsilon V_b/4\pi eW_b$ and $\Sigma_{-,0}^d - \Sigma_{+,0}^d = \varepsilon(V_b - V_d)/4\pi eW_b$, respectively, where the quantities with the index “0” are the electron and hole densities in the immediate vicinity of the source and drain contacts, we arrive at the following equation:

$$\sinh\left(\frac{\varepsilon_F^s}{k_B T}\right) = \exp\left(\frac{\Delta}{2k_B T}\right)$$

$$\times \left[\frac{\varepsilon}{16\sqrt{\pi}} \frac{eV_b}{\sqrt{\Delta k_B T}} \left(\frac{d}{W_b}\right) \left(\frac{\hbar v}{e^2}\right) \right], \quad (7)$$

$$\sinh\left(\frac{\varepsilon_F^d}{k_B T}\right) = \exp\left(\frac{\Delta - 2eV_d}{2k_B T}\right)$$

$$\times \left[\frac{\varepsilon}{16\sqrt{\pi}} \frac{e(V_b - V_d)}{\sqrt{\Delta k_B T}} \left(\frac{d}{W_b}\right) \left(\frac{\hbar v}{e^2}\right) \right]. \quad (8)$$

When $V_b = V_g = V_d = 0$, one obtains $\varepsilon_F^s = \varepsilon_F^d = 0$, so that the electron and hole densities are equal to their thermal value [17]

$$\Sigma_T = \frac{2\sqrt{\Delta k_B T}}{\sqrt{\pi}\hbar d v} \exp\left(-\frac{\Delta}{2k_B T}\right). \quad (9)$$

For the effective operation of a GNR-FET with the n-type channel, the electron densities in the sections of the channel should be reasonably high (to provide necessary conductivity of these sections). This requires the application of a sufficiently high back gate voltage. If

$$\exp\left(-\frac{\Delta}{2k_B T}\right), \ll \frac{V_b}{V_F}, \frac{(V_b - V_d)}{V_F} < 1, \quad (10)$$

where

$$V_F = \frac{\sqrt{\Delta k_B T}}{e} \left[\frac{8\sqrt{\pi}}{\varepsilon} \left(\frac{W_b}{d}\right) \left(\frac{e^2}{\hbar v}\right) \right], \quad (11)$$

as follows from Eqs. (7) and (8), $\varepsilon_F^s, \varepsilon_F^d \gg k_B T$, and

$$\begin{aligned} \varepsilon_F^s &\simeq \frac{\Delta}{2} + k_B T \ln\left(\frac{V_b}{V_F}\right), \\ \varepsilon_F^d &\simeq \frac{\Delta}{2} + k_B T \ln\left(\frac{V_b - V_d}{V_F}\right). \end{aligned} \quad (12)$$

At V_b and $(V_b - V_d)$ satisfying inequality (10), the electron gas is nondegenerate and the electron density markedly exceeds its thermal value as well as the density of holes. In the case under consideration, the electron density in the pertinent sections of the channel, as follows from Eqs. (6) and (12), are given by

$$\begin{aligned} \Sigma_{-}^s &\simeq \frac{\varepsilon V_b}{4\pi eW_b} \exp\left(\frac{e\varphi}{k_B T}\right), \\ \Sigma_{-}^d &\simeq \frac{\varepsilon(V_b - V_d)}{4\pi eW_b} \exp\left[\frac{e(\varphi - V_d)}{k_B T}\right]. \end{aligned} \quad (13)$$

Since at $V_b > 0$, the electron density markedly exceeds the hole density, we can neglect Σ_h in the right-hand side of Eq. (2). The case when the hole gas under the top gate becomes essential (at very high top gate voltages) will be discussed in the following (in Section V). Considering the relationships between the electron density and the electric potential, from Eq. (2) one can arrive at the following equations governing the potential distribution in the active region:

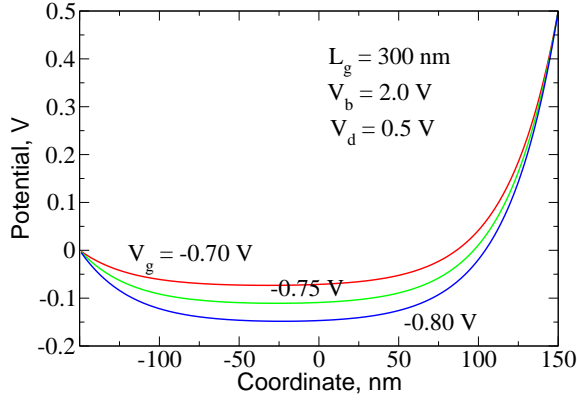


FIG. 2: Spatial distributions of the potential at different top gate

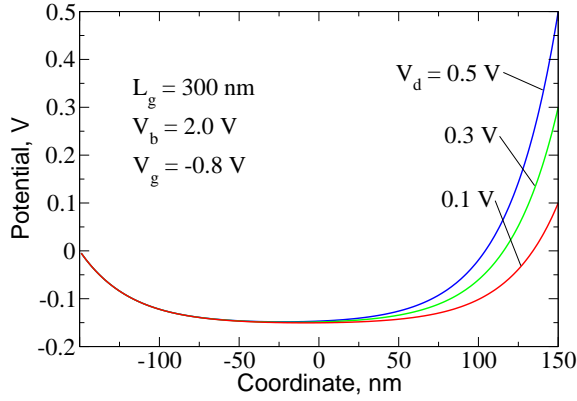


FIG. 3: Spatial distributions of the potential at different drain voltages.

$$\frac{d^2 \varphi}{dx^2} - \frac{3}{W_b W_g} \varphi = -\frac{3(V_b/W_b + V_g/W_g)}{(W_b + W_g)} + \frac{3}{(W_b + W_g)} \frac{V_b}{W_b} \exp\left(\frac{e\varphi}{k_B T}\right), \quad (14)$$

$$\frac{d^2 \varphi}{dx^2} - \frac{3}{W_b W_g} \varphi = -\frac{3(V_b/W_b + V_g/W_g)}{(W_b + W_g)} + \frac{3}{(W_b + W_g)} \frac{(V_b - V_d)}{W_b} \exp\left[\frac{e(\varphi - V_d)}{k_B T}\right]. \quad (15)$$

The exponential dependences in the right-hand sides of Eqs. (14) and (15) are valid provided that inequality (10) is satisfied, in particular, if the electron gas is nondegenerate. The threshold value of the back gate voltage, at which the degeneration of the electron gas occurs, can be estimated as $V_b \simeq V_F$.

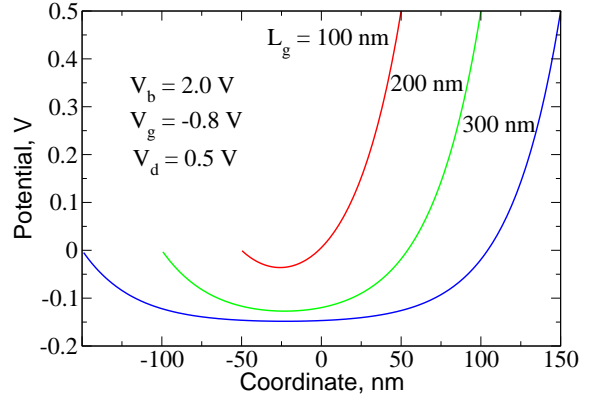


FIG. 4: Spatial distributions of the potential in GNR-FETs with different gate lengths.

B. Potential distributions at low top-gate voltages

When the top gate is negative ($V_g < 0$) and its absolute value $|V_g|$ is sufficiently small, the modulus of the potential $|\varphi|$ can be not that large. In this case, one can linearize Eqs. (14) and (15) and present these equations in the following form:

$$\frac{d^2 \varphi}{dx^2} - \frac{3}{W_b W_g} \left[1 + \frac{W_g}{(W_b + W_g)} \frac{eV_b}{k_B T} \right] \varphi = -\frac{3V_g}{(W_b + W_g)W_g}, \quad (16)$$

$$\frac{d^2 \varphi}{dx^2} - \frac{3}{W_b W_g} \left[1 + \frac{W_g}{(W_b + W_g)} \frac{e(V_b - V_d)}{k_B T} \right] \varphi = -\frac{3(V_g/W_g - V_d/W_b)}{(W_b + W_g)}. \quad (17)$$

Equations (16) and (17) should be solved taking into account Eq. (3) and the matching of φ and $d\varphi/dx$ at a certain point $x = x_m$ (such that $-L_g/2 < x_m < L_g/2$), at which φ reaches a minimum. Such a minimum definitely exist when $V_g < 0$. At $V_d = 0$, Eqs. (16) and (17) yield

$$\varphi \simeq \frac{V_g W_b}{(W_b + W_g)} \frac{\left[1 - \frac{\cosh(x/\lambda)}{\cosh(L_g/2\lambda)} \right]}{\left[1 + \frac{W_g}{(W_b + W_g)} \frac{eV_b}{k_B T} \right]}. \quad (18)$$

where

$$\lambda = \Lambda / \sqrt{1 + \frac{W_g}{(W_b + W_g)} \frac{eV_b}{k_B T}} \simeq \Lambda / \sqrt{\frac{W_g}{(W_b + W_g)} \frac{eV_b}{k_B T}}$$

is the effective screening length and $\Lambda = \sqrt{W_b W_g/3}$. At $V_d = 0$, as follows from Eq. (18), the function φ exhibits a minimum $\varphi = \varphi_{m0}$ at $x = 0$ with

$$\begin{aligned} \varphi_{m0} &\simeq \frac{V_g W_b}{(W_b + W_g)} \frac{\left[1 - \frac{1}{\cosh(L_g/2\lambda)}\right]}{\left[1 + \frac{W_g}{(W_b + W_g)} \frac{eV_b}{k_B T}\right]} \\ &\simeq \frac{V_g W_b k_B T}{V_b W_g e}. \end{aligned} \quad (19)$$

Here, we have taken into account that normally $V_b \gg k_B T/e$ and $L_g \gg \lambda$ (with $\lambda < \Lambda$).

At reasonable values of the drain voltages V_d , the variation of $\varphi_m - \varphi_{m0}$ is equal to $V_d/2 \cosh(L_g/2\lambda) \ll V_d$, i.e., is very small due to $\cosh(L_g/2\lambda) \gg 1$ and can be disregarded, so that

$$\varphi_m \simeq \varphi_{m0} \simeq \frac{V_g W_b k_B T}{V_b W_g e}. \quad (20)$$

Comparing $e|\varphi_m|$ given by Eq. (20) with $k_B T$, we find that Eqs. (16) - (19) are valid when $|V_g| \lesssim V_b W_g/W_b$

C. Potential distributions at high top-gate voltages

At high back gate voltages, the quantity λ playing the role of the screening length is rather small. In this case, the length of the regions near the points $x = \pm L_g/2$, in which the potential changes from $\varphi = 0$ to $|\varphi| > k_B T$ and from $\varphi = V_d$ to $|\varphi - V_d| > k_B T$, is small in comparison with the top gate length L_g . In such short regions near $x = \pm L_g/2$, the potential distribution can still be describe by Eq. (18). However, in a significant part of the active region the electron charge, which is in such a situation exponentially small, can be disregarded and the last (exponential) terms in Eqs. (14) and (15) can be omitted. Taking this into account, at high top gate voltages, Eqs. (14) and (15) in the central region can be presented in the following form:

$$\frac{d^2 \varphi}{dx^2} - \frac{3}{W_b W_g} \varphi = -\frac{3(V_g/W_g + V_b/W_b)}{(W_b + W_g)}. \quad (21)$$

Solving Eqs. (21) still using boundary conditions given by Eq. (3), we arrive at

$$\begin{aligned} \varphi &= \left(V_g + V_b \frac{W_g}{W_b}\right) \frac{W_b}{(W_b + W_g)} \left[1 - \frac{\cosh(x/\Lambda)}{\cosh(L_g/2\Lambda)}\right] \\ &\quad + V_d \frac{\sinh[(x + L_g/2)/\Lambda]}{\sinh(L_g/\Lambda)}, \end{aligned} \quad (22)$$

At $V_d = 0$, φ exhibits a minimum at $x = 0$ and

$$\varphi_{m0} \simeq \left(V_g + V_b \frac{W_g}{W_b}\right) \frac{W_b}{(W_b + W_g)} \left[1 - \frac{1}{\cosh(L_g/2\Lambda)}\right]. \quad (23)$$

In the limit $L_g \gg \Lambda$, the potential in the center of the channel given by Eq. (22) coincides with that obtained in the gradual channel approximation. However, in real GNR-FET structures, L_g can be comparable with Λ . In this case, the terms dependent on L_g can be important (in contrast to the case of low gate voltages considered in the previous subsection). At reasonable values of the drain voltage V_d (sufficiently small compared to V_b), Eq. (22) yields

$$\begin{aligned} \varphi_m &\simeq \left(V_g + V_b \frac{W_g}{W_b}\right) \frac{W_b}{(W_b + W_g)} \left[1 - \frac{1}{\cosh(L_g/2\Lambda)}\right] \\ &\quad + \frac{V_d}{2 \cosh(L_g/2\Lambda)}. \end{aligned} \quad (24)$$

Figures 2 and 3 show examples of the spatial distributions (along the channel, i.e., in the x -direction) of the electric potential in the active region (under the top gate) calculated for a GNR-FET with $W_b = 100$ nm, $W_g = 30$ nm, and $L_g = 300$ nm at the back gate voltage $V_b = 2.0$ V, assuming different values of the top gate voltage V_g and the drain voltage V_d . As seen from Fig. 2, the potential distribution markedly sags and the height of the barrier for electrons near the center increases with increasing absolute value of the top gate potential $|V_g|$. Figure 3 demonstrates, in particular, that in the GNR-FET with chosen parameters the minimum value of the potential φ_m and, hence, the height of the barrier $-e\varphi_m$ for the electrons propagating from the source are virtually insensitive to the drain voltage. In contrast, the potential barrier $e(V_d - \varphi_m)$ for the electrons propagating from the drain increases linearly with increasing V_d . Figure 4 shows the spatial distributions of the electric potential calculated for the GNR-FETs with different gate lengths L_g .

The approach used in this subsection is valid when $e|\varphi_m| \gg k_B T$, i.e., when $|V_g| - V_b W_g/W_b \gg k_B T(W_b + W_g)/eW_b \sim k_B T/e$.

In the limit $L_g \gg \Lambda > \lambda$ the equations for φ_m obtained above (in particular Eq. (24)) coincide with those obtained using the gradual channel approximation.

IV. CALCULATION AND ANALYSIS OF CURRENT-VOLTAGE CHARACTERISTICS

Considering that the source-drain current is determined by the electrons overcoming the potential barrier under the top gate, one can use the following formula for the density of this current (per unit length):

$$J = \frac{2e}{\pi \hbar d} \left(\int_{p_m^s}^{\infty} dp v_p f_p^s - \int_{p_m^d}^{\infty} dp v_p f_p^d \right). \quad (25)$$

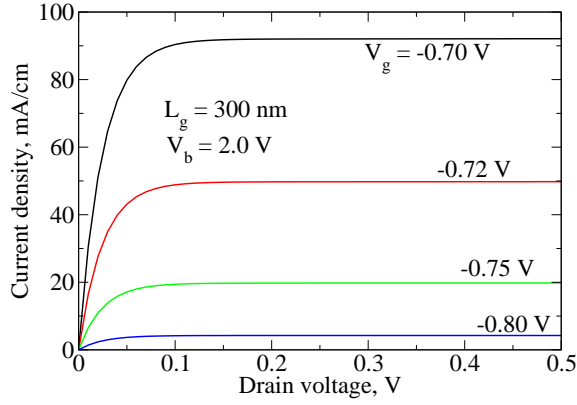


FIG. 5: The source-drain current density versus drain voltage dependencies at fixed back gate voltage ($V_b = 2.0$ V) and different top gate voltages V_g .

Here,

$$v_p = \frac{d\varepsilon_{p,0}^+}{dp} = v^2 \frac{p}{\sqrt{v^2 p^2 + \Delta^2/4}}$$

is the velocity of the electron with momentum p in the lowest subband of the nanoribbon conduction band and p_m^s and p_m^d are the momenta of the electrons with the energies $e|\varphi_m|$ and $e(|\varphi_m| + V_d)$, respectively. We have taken into account that the nanoribbon array is dense: $d_s \ll d$. Integrating in Eq. (26), we arrive at

$$J = v \left(\frac{\varkappa}{2\pi^{3/2} W_b} \right) \sqrt{\frac{k_B T}{\Delta}} \exp\left(\frac{e\varphi_m}{k_B T}\right) \times \left[V_b - (V_b - V_d) \exp\left(-\frac{eV_d}{k_B T}\right) \right] \quad (26)$$

with φ_m given by Eq. (20) at low top gate voltages and by Eq. (24) at moderate and high voltages, respectively. Equation (26) corresponds to the average thermal electron velocity $v_T = v\sqrt{4k_B T/\pi\Delta}$. One can see that the thermal electron velocity as well as the pre-exponential factor in the formula for the current depend on the band gap. This is due to the dependence on the gap of the electron dispersion and the electron velocity.

A. Current versus drain voltage

The dependence of the source-drain current on the drain voltage is associated with the dependence of φ_m on this voltage given by Eqs. (20) and (24) and the voltage dependence of the last factor in the right-hand side of Eq. (26). At low top gate voltages ($|V_g| \lesssim V_b W_g/W_b$), using Eqs. (20) and (26), we obtain

$$J \propto \left[V_b - (V_b - V_d) \exp\left(-\frac{eV_d}{k_B T}\right) \right], \quad (27)$$

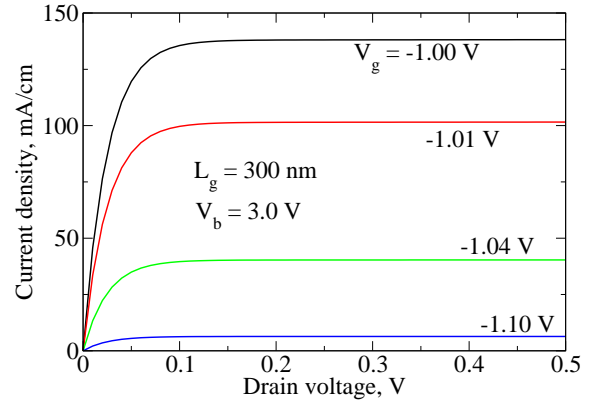


FIG. 6: The same as in Fig. 5 but for $V_b = 3.0$ V.

i.e.,

$$J \propto V_d \quad (28)$$

if $V_d \lesssim k_B T/e$, and

$$J = \text{const} \quad (29)$$

if $k_B T/e \ll V_d \lesssim V_b W_g/W_b$.

At moderate and high top gate voltages when φ_m is given by Eq. (24), we arrive at the following dependence

$$J \propto \exp\left[\frac{eV_d}{2k_B T \cosh(L_g/2\Lambda)}\right] \times \left[V_b - (V_b - V_d) \exp\left(-\frac{eV_d}{k_B T}\right) \right]. \quad (30)$$

At $V_d \lesssim k_B T/e$, Eq. (30) yields the same linear dependence on the drain voltage as that described by Eq. (28). When $V_d \gg k_B T/e$, one obtains

$$J \propto \exp\left[\frac{eV_d}{2k_B T \cosh(L_g/2\Lambda)}\right]. \quad (31)$$

The latter dependence resembles the dependence given by Eq. (29), but with the substitution of λ by Λ . Since $\lambda \ll \Lambda$, the source-drain current at moderate and high top gate voltages is a less steeper function of the drain voltage than that at low top gate voltages (compare Eqs. (29) and (31)).

The J versus V_d dependences for a GNR-FET with $L_g = 300$ nm at the back gate voltages $V_g = 2$ V and $V_g = 3$ V calculated for the different top gate voltages V_g are shown in Figs 5 and 6. Here, as in the previous and consequent figures, we assumed that $\Delta = 0.4$ eV, $\varkappa = 4$, $W_b = 100$ nm, $W_g = 30$ nm, and $T = 300$ K. Since the gate voltages were set to be relatively high ($V_b, |V_g| \gg k_B T/e \simeq 0.025$ V), Eqs. (24) and (26) were used for the calculations.

As seen from Figs. 5 and 6, the source-drain current as a function of the drain voltage in a GNR-FET with

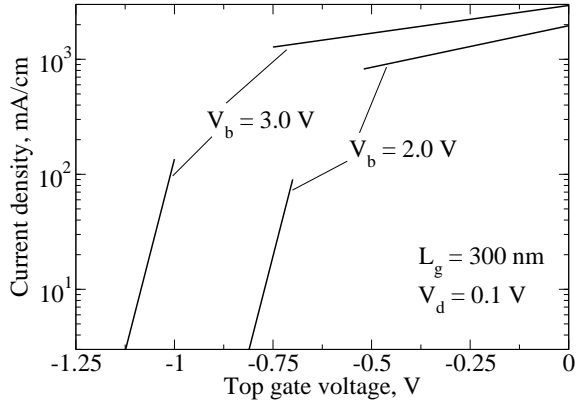


FIG. 7: The source-drain current density as a function of the top gate voltage at different back gate voltages.

relatively long gate ($L_g = 300$ nm) exhibits saturation starting rather low drain voltages. This is a consequence of very weak sensitivity of the potential barrier for the electrons propagating from the source to the drain voltage.

B. Current versus gate voltages

As follows from Eqs. (20), (24), and (26), the source-drain current as a function of the top gate voltage is described by the following relations:

$$J \propto \exp\left(\frac{V_g W_b}{V_b W_g}\right) \quad (32)$$

at $|V_g| \lesssim V_b W_g / W_b$, and

$$J \propto \exp\left[\frac{eV_g}{k_B T} \frac{W_b}{(W_b + W_g)} \left(1 - \frac{1}{\cosh(L_g/2\Lambda)}\right)\right] \quad (33)$$

at $|V_g| > V_b W_g / W_b$.

Figures 5 and 6 show the transformation of the J vs V_d dependences with varying top gate voltage in the range of the latter $|V_g| > V_b W_g / W_b$. These figures confirm a strong sensitivity of the source-drain current to the gate voltages. As follows from Eqs. (32) and (33), the dependence of the source-drain current on the top gate voltage is much steeper in the range high top gate voltages $|V_g| \gtrsim V_b W_g / W_b$ than at $|V_g| \lesssim V_b W_g / W_b$, i.e., when the central region of the channel becomes essentially depleted. Figure 7 shows the J versus V_g characteristics obtained using Eq. (26) in which φ_m was determined by Eq. (20) (for small $|V_g|$) and by Eq. (24) (for large $|V_g|$), respectively.

The ratio the transconductance $g = \partial J / \partial V_g$ to the source-drain current J at high top gate voltages $|V_g| > V_b W_g / W_b$ to the same ratio at low top gate voltage $|V_g| <$

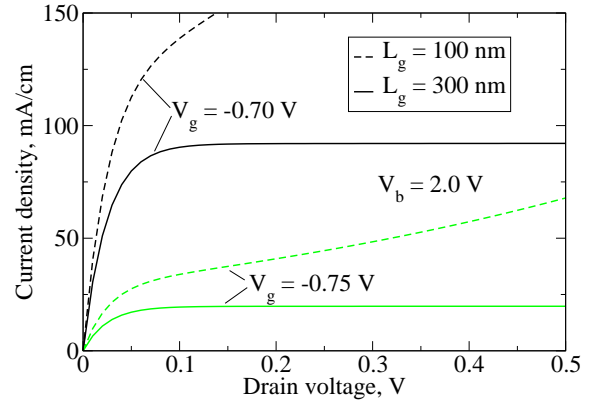


FIG. 8: The source-drain current density as a function of the drain voltage in GNR-FETs with different gate lengths at different top gate voltages: solid lines - $L_g = 300$ nm ("long" gate) and dashed lines - $L_g = 100$ nm ("short" gate).

$V_b W_g / W_b$ is given by

$$\left(\frac{g}{J}\right)_{high} / \left(\frac{g}{J}\right)_{low} \simeq \frac{eV_b}{k_B T} \frac{W_g}{(W_b + W_g)} \gg 1. \quad (34)$$

The source-drain current versus the back gate dependence at high top gate and drain voltages is given by

$$J \propto V_b \exp\left[\frac{eV_b}{k_B T} \frac{W_g}{(W_b + W_g)} \left(1 - \frac{1}{\cosh(L_g/2\Lambda)}\right)\right]. \quad (35)$$

The source-drain current increases with increasing back gate voltage due to the pertinent increase in the electron density in all regions of the channel.

C. Short-gate effects

As follows from the above formulas, the current-voltage characteristics exhibits pronounced dependence on the top gate length. This can be attributed to an essential dependence of the height of the potential barrier for the electrons propagating from the source on the top gate length (as, in particular, seen from Fig. 4) and on the drain voltage. As a result, the J versus V_d dependence (see Eqs. (29) and (31)) becomes markedly steeper when the top gate length decreases, particularly, when the latter becomes comparable with Λ (or λ).

In particular, as seen from Eqs. (29) and (31), in a GNR-FET with a long top gate, the source-drain current saturates when V_d becomes larger than $k_B T / e$, whereas in a GNR-FET with L_g comparable with Λ , the source-drain current markedly increases with increasing V_d even at rather large values of the latter. This is confirmed by the current-voltage characteristics calculated for GNR-FETs with a "long" ($L_g = 300$ nm) and a "short" ($L_g = 100$ nm) top gates shown in Fig. 7.

V. DISCUSSION

A. GNR-FET in common-drain circuit

Above we considered the case of GNR-FETs in the common-source circuit (see Fig. 1), so that the voltage between the back gate and the source and between the top gate and the source are equal to V_b and V_g , respectively. In the case of GNR-FETs in the common-drain circuit, the voltages V_b and V_g are applied between that back gate and the drain and between the top gate and drain. In such a situation, in the above formulas one needs to replace V_b by $V_b + V_d$ and V_g by $V_g + V_d$. In this case, Eqs. (24) and (26) should be replaced by the following equations:

$$\varphi_m \simeq \left[\frac{(V_g + V_b W_g / W_b) W_b}{(W_b + W_g)} + V_d \right] \left[1 - \frac{1}{\cosh(L_g / 2\Lambda)} \right] + \frac{V_d}{2 \cosh(L_g / 2\Lambda)} \quad (36)$$

and

$$J = v \left(\frac{\varkappa}{2\pi^{3/2} W_b} \right) \sqrt{\frac{k_B T}{\Delta}} \exp\left(\frac{e\varphi_m}{k_B T}\right) \times \left[V_b + V_d - V_b \exp\left(-\frac{eV_d}{k_B T}\right) \right]. \quad (37)$$

The main difference between the GNR-FET current-voltage characteristics in the common source circuit and in the common drain circuit is that in the latter case the source-drain current is a rather steep function of the drain voltage even at $V_d \gg k_B T / e$. Indeed, as seen from Eq. (31), in the GNR-FETs with $L_g \gg \Lambda$, the current tends to saturation in the voltage range $V_d \gg k_B T / e$. However, Eqs. (36) and (37) valid in the case of the common drain circuit, give rise to an exponential voltage dependence, which at $V_d \gg k_B T / e$ becomes as follows:

$$J \propto \exp\left(\frac{eV_d}{k_B T}\right). \quad (38)$$

B. Role of holes

At elevated top gate and drain voltages, the top of the valence band in the central section of the channel can become higher than the Fermi levels in the side sections. In this case, a significant amount of holes can occupy the central section of the channel, so that a p -region can be formed in this section. Such an effect can occur when $e|\varphi_m| > \Delta/2 + \varepsilon_F^s$ or $e|\varphi_m| + eV_d > \Delta/2 + \varepsilon_F^d$. Since in the case of nondegenerate electron gas in the channel $\varepsilon_F^s, \varepsilon_F^d < \Delta/2$, the condition, at which the hole gas under the top gate might be essential, can be presented as

$|\varphi_m|, |\varphi_m| + V_d \gtrsim \Delta/e$. As an example, assuming that $V_d \ll V_b$ and setting $\Delta = 0.4$ eV, $W_g = 0.3W_b$, and $V_b = 2 - 3$ V one obtains that the hole effects can be essential if $|V_g| \gtrsim 1$ V. It implies that the hole gas can affect the GNR-FET characteristics at elevated but realistic values of the top gate voltages. The hole charge under the top gate results in slowing down of the decrease of the source-drain current with increasing $|V_g|$. At higher top gate and/or drain voltages, the tunneling between the n -regions in the channel not covered by the top gate and the p -region under this gate becomes tangible. As a result, the source-drain current can increase dramatically. [6, 7, 8, 9, 10] The tunneling current between in the degenerate n - and p -sections in the channel of a graphene FET was studied previously. [6, 10] In the GNR-FETs with a marked energy band gap and a nondegenerate electron gas in the side sections of the channel (n - regions), the tunneling current can become essential at fairly high voltages. Indeed, taking into account that the probability of the interband tunneling between the subbands with $n = 1$ is given by [7, 8] $t_t = \exp(-\pi^3 \hbar v / e E_m d^2)$, where E_m is the characteristic electric field in the n-p and p-n junctions arisen due to the population of the central section of the channel by holes. This field we estimate as $E_m = |\varphi_m| / \Lambda = |\varphi_m| \sqrt{3 / W_b W_g}$ in the n-p junction and $E_m = (|\varphi_m| + V_d) \sqrt{3 / W_b W_g}$ in the p-n junction. Using the above estimates, one can find that the tunneling might be essential at the values of $|\varphi_m|$ and/or V_d exceeding the characteristic tunneling voltage $V_t = (\pi/4\sqrt{3}) \Delta^2 \sqrt{W_b W_g} / e \hbar v$. Setting $W_b = 100$ nm, $W_g = 30$ nm, and $\Delta = 0.4$ eV, we obtain $V_t \simeq 6.4$ V. If $V_d \ll V_b$ and $V_b = 2 - 3$ V, this implies that the interband tunneling might become significant at $|V_g| \gtrsim 9$ V. However, the quantitative study of the tunneling effects in GNR-FETs with narrower energy gap, in which the tunneling can occur at moderate voltages, requires a separate careful consideration which is beyond the scope of this paper.

C. Main limitations of the model

The validity of the device model used above is limited by the following:

(1) Applicability of the weak nonlocality approximation which requires that the parameter $\delta = [(W_b^3 + W_g^3) / 45(W_b + W_g)] \mathcal{L}^2 \ll 1$. This problem might arise only in the case of GNR-FETs with rather short top gate length when the terms in Eqs. (23) and (24) containing $\cosh(L_g / 2\Lambda)$ are essential. In the most interesting case, as follows from Eq. (22), $\mathcal{L} = \sqrt{W_b W_g} / 3$. In such a case, $\delta = [(W_b^3 + W_g^3) / 15(W_b + W_g)] W_b W_g \ll 1$. In particular, the latter yields $\delta = 1/15 \simeq 0.067$ if $W_b = W_g$ and $\delta \simeq 0.175$ if $W_g / W_b = 0.3$. Using the Poisson equation in the weak nonlocality approximation and retaining the next term in the expansion of the two-dimensional Poisson equation over δ , one can find that the value $L_g / 2\Lambda$ in Eq. (24) should be replaced by fairly close

value $L_g\sqrt{(1+\delta)}/2\Lambda \simeq L_g(1+\delta/2)/2\Lambda$.

(2) Not excessively high back gate voltages ($V_b < V_F$). This is due an assumption that the electron gas in the channel is nondegenerate. Setting $d = 3$ nm, $W_b = 100$ nm, $ae = 4$, $v = 10^8$ cm/s, $\Delta = 0,4$ eV, and $T = 77 - 300$ K, we obtain the following estimate $V_F \simeq 14.0-27.6$ V. This estimate, as well as the smallness of $\exp(-\Delta/k_B T)$, imply that inequality (10) is satisfied and, hence, Eqs. (14) and (15) are valid in fairly wide range of the back gate voltages, which definitely covers the range of voltages used in real devices.

(3) Not excessively high top gate and drain voltages, so that the effects associated with holes under the top gate can be disregarded (see the previous Subsection).

(4) The device structures with relatively weak scattering of electrons on impurities and phonons in the active region of the channel. The electron scattering in this region can give rise to a decrease in the pre-exponential factor in the formula for the source-drain current in comparison to that in Eq. (26). However, the main voltage dependences obtained above and those which can be found using the drift-diffusion model of the electron transport in the active region of the channel should be essentially the same. In some sense, the situation is similar to that which occurs in the theory of the Schottky diodes and conventional p-n- junctions when the so-called thermionic and diffusion models are compared [14, 15].

One can see that the device model used above adequately describes the operation of GNR-FETs with realistic parameters at reasonable applied voltages.

VI. CONCLUSIONS

In conclusion, we developed an analytical device model for GNR-FETs. The GNR-FET current-voltage characteristics, i.e., the dependencies of the source-drain current versus the drain voltage as well as the back gate and top gate voltages, were calculated for the devices with different geometric parameters (thicknesses of the gate layers and the top gate length) using this model. In particular, we showed that shortening of the top (controlling) gate gives rise to a substantial transformation of the GNR-FET current-voltage characteristics (the short-gate effect). The model can be used for the GNR-FET optimization.

VII. ACKNOWLEDGMENT

The work was supported by CREST, the Japan Science and Technology Agency, Japan.

[*] Electronic address: v-ryzhii@u-aizu.ac.jp

- [1] C. Berger, Z. Song, T. Li, X. Li, A.Y. Ogbazhi, R. Feng, Z. Dai, A. N. Marchenkov, E. H. Conrad, P. N. First, and W. A. de Heer, *J. Phys. Chem.* **108**, 19912 (2004).
- [2] K. S. Novoselov, A. K. Geim, S. V. Morozov, D. Jiang, M. I. Katsnelson, I. V. Grigorieva, S. V. Dubonos, and A. A. Firsov, *Nature* **438**, 197 (2005).
- [3] A. K. Geim and K. S. Novoselov, *Nat. Mater.* **6**, 183 (2007).
- [4] B. Obradovich, R. Kotlyar, F. Heinz, P. Matagne, T. Rakshit, M. D. Giles, M. A. Stettler, and D. E. Nikonov, *Appl. Phys. Lett.* **88**, 142102 (2006).
- [5] J. Hass, R. Feng, T. Li, X. Li, Z. Zong, W. A. de Heer, P. N. First, E. H. Conrad, C. A. Jeffrey, and C. Berger: *Appl. Phys. Lett.* **89**, 143106 (2006).
- [6] B. Huard, J. A. Sulpizio, N. Stander, K. Todd, B. Yang, and D. Goldhaber-Gordon, *Phys. Rev. Lett.* **98**, 236803 (2007).
- [7] V. V. Cheianov and V. I. Fal'ko, *Phys. Rev. B* **74**, 041403 (2006).
- [8] A. Ossipov, M. Titov, and C. W. J. Beenakker, *Phys. Rev. B* **75**, 241401 (2007).
- [9] L. M. Zhang and M. M. Fogler: arXiv:cond-mat/0708.0892.
- [10] V. Ryzhii, M. Ryzhii, and T. Otsuji, *Appl. Phys. Express*, **1**, 000 (2008)
- [11] Z. Chen, Y.-M. Lin, M. J. Rooks, and P. Avouris, *Physica E* **40**, 228 (2007).
- [12] A. A. Sukhanov and Yu. Ya. Tkach, *Sov. Phys. Semicond.* **18**, 797 (1984).
- [13] V. I. Ryzhii and I. I. Khmyrova, *Sov. Phys. Semicond.* **22**, 807 (1988).
- [14] M. Shur, *Physics of Semiconductor Devices* (Prentice Hall, New Jersey, 1990).
- [15] S. M. Sze, *Physics of Semiconductor Devices* (Wiley, New York, 1981).
- [16] A. O. Govorov, V. M. Kovalev, and A. V. Chaplik, *JETP Lett.* **70**, 488 (1999).
- [17] T. Fang, A. Konar, H. Xing, and D. Jena, *Appl. Phys. Lett.* **91**, 092109 (2007).